A novel equivalent modeling method combined with the splice-electrochemical polarization model and prior generalized inverse least-square parameter identification for UAV lithium-ion batteries.

PENG, J., SHI, H., WANG, S., WANG, L., FERNANDEZ, C., XIONG, X. and BOBOBEE, E.D.

2022

ORIGINAL ARTICLE

A novel equivalent modeling method combined with the splice-electrochemical polarization model and prior generalized inverse least-square parameter identification for UAV lithium-ion batteries

Jiawei Peng[1] | Haotian Shi[1] | Shunli Wang[1] | Liping Wang[1,2] | Carlos Fernandez[3] | Xin Xiong[1,4] | Bobobee Etse Dablu[1]

[1]Department of Information Engineering, Southwest University of Science and Technology, Mianyang, China

[2]Department of Mechanical Engineering, Tsinghua University, Beijing, China

[3]Department of Pharmacy and Life Sciences, Robert Gordon University, Aberdeen, UK

[4]Department of Automation, University of Science and Technology of China, Hefei, China

Correspondence
Shunli Wang, No. 59, Middle Section of Qinglong Avenue, Fucheng District, 621010 Mianyang City, Sichuan Province, China.
Email: wangshunli@swust.edu.cn

Funding information
National Natural Science Foundation of China, Grant/Award Number: 61801407

Abstract

The accuracy of lithium-ion battery state estimation is critical to the safety of unmanned aerial vehicles (UAVs). In this paper, aiming at the high-fidelity modeling of the UAV lithium-ion battery, a splice-electrochemical polarization model (S-EPM) for UAV lithium-ion battery is constructed by combining the traditional electrochemical model with the equivalent circuit model, which greatly improved the accuracy of the battery modeling. In addition, a novel prior generalized inverse least-squares algorithm is proposed. Also, based on this algorithm, the full-parameter identification and multicondition error analysis of the S-EPM are realized based on this algorithm. Finally, a targeted complex discharge rate test and a full-function charge–discharge test were designed to further verify the applicability of the S-EPM to complex conditions. The experimental results show that the voltage error of the model under each working condition is 5.50 and 3.0 mV, and the maximum percentage error ratio is 0.20% and 0.07%. This experiment can provide a theoretical basis for the combination of the electrochemical model and equivalent circuit model and the accurate estimation of internal state variables of lithium-ion batteries.

KEYWORDS
improve the Nernst model, lithium-ion batteries, parameter identification, prior generalized inverse least square, splice-electrochemical polarization model

1 | INTRODUCTION

The power battery system is one of the most important components of an unmanned aerial vehicle (UAV), which has a great impact on the performance and safety of the whole aircraft.[1] The lithium-ion battery has become the most widely used power battery for aircraft due to its excellent performance. For UAVs, the high-performance battery management system can not only ensure the timeliness of the drone flight but also extend

the service life of the drone's lithium battery. The strong nonlinear characteristics of the UAV lithium battery make it difficult to build a high-fidelity model of the UAV lithium battery. In addition, due to the unique complex working environment of UAVs, it is also a huge challenge to achieve a high-precision estimation of the state of charge (SoC) of UAV lithium batteries.[2] Therefore, the establishment of a high-fidelity lithium-ion battery model is the most important step to achieving efficient management of lithium-ion batteries.[3]

Many scholars have carried out related research on the modeling of the equivalent circuit of lithium-ion batteries. Meng et al.[4] proposed a nonlinear model to accurately describe the external characteristics of lithium-ion batteries and conducted experiments on LiFePO$_4$ batteries to prove the effectiveness of the model. Amiribavandpour et al.[5] improved the electrochemical modeling theory and improved the precision of battery pack temperature prediction, but the temperature range considered was not wide enough and other influencing factors were not considered. Zhou et al.[6] improved the adaptive particle swarm optimization-simulated annealing method, completed the parameter identification of the lithium-ion battery adaptive model, and the results showed a good convergence rate. Nejad et al.[7] combined the equivalent circuit model to build the real-time state estimation of lithium-ion batteries. Ferahtia et al.[8] proposed a model optimal parameter identification strategy, which has better identification ability than other optimization algorithms. Li et al.[9] established an electrochemical lithium-ion battery model in a wide temperature range and verified the model in the temperature range of −20°C to 45°C, but the experimental verification conditions were too simple. Yang et al.[10] realized the design of an adaptive parameter identification method for the estimation of the SoC of lithium-ion batteries based on the improved extended Kalman filter. Hu and Wang[11] studied the parameter identification of the dual-time-scale battery model and its application in battery state estimation, which improved the robustness of the battery system. Jun et al.[12] constructed the impedance model of the porous electrode of the lithium-ion battery and carried out a mathematical representation of the model's order reduction space. Li et al.[13] realized the dynamic modal analysis and physical parameter identification of lithium-ion batteries based on a simplified electrochemical model, but the external factors considered were relatively single and failed to fully consider the factors affecting aging.

Given the necessity and urgent needs of lithium battery equivalent modeling, in addition to the above-mentioned research by related scholars, there are also experts in many fields who have conducted systematic research on battery modeling and parameter identification and have achieved good results. Jiang et al.[14] established an equivalent mechanical model of a lithium-ion battery based on the stacking theory, providing a new idea for high-fidelity battery modeling. Dai et al.[15] proposed a novel separation time scale adaptive model parameter identification strategy, which improved the consistency of model parameters. Wang et al.[16] established an equivalent model of a fully charged lithium-ion battery based on the internal electrochemical process of the battery, which greatly improved the SoC estimation performance in the low-range area, but the performance in the high-range area was not significant. Tanaka et al.[17] studied the transient voltage distribution simulation method based on the internal equivalent circuit, which improved the simulation efficiency of the battery equivalent circuit model. Zhu et al.[18] proposed a new recursive restricted total least-squares algorithm, combined with the unscented Kalman filter to achieve a joint estimation of the lithium-ion battery model parameters and SoC, the average absolute error of SoC and the convergence time is limited to 1.2% and 88 s, respectively. Jenkins et al.[19] designed a fast adaptive observer for the battery management system, which can quickly estimate the internal state of the battery management system under certain operating conditions, but this design does not consider the changeable battery application environment. Wu et al.[20] On the basis of the study of parameter identification of lithium-ion battery models, an analysis of the increase in voltage without an open circuit was carried out to improve the precision of parameter estimation. Wei et al.[21] analyzed and summarized different lithium-ion battery integration models and SoC estimation methods, providing a theoretical basis for the establishment of high-fidelity models and high-precision battery state estimation. Kornas et al.[22] proposed a multicriteria optimization strategy that needs to be considered in the production of lithium-ion batteries, which improves the production efficiency of batteries. Park et al.[23] realized the SoC/capacity complementary cooperative estimation of the power system based on the discrete variational derivative and the double extended Kalman filter algorithm, providing a theoretical and experimental basis for the SoC estimation method of lithium-ion batteries in this way. Tian et al.[24] established a lithium-ion battery capacity decay mechanism modeling and kept the root-mean-square error (RMSE) and average absolute error of the calculated voltage within 38 and 51 mV, respectively. The uncertainty and stability of parameters of the lithium-ion battery model and SoC estimation are analyzed by Yuan et al.[25] Xie et al.[26] proposed an enhanced online temperature estimation method for

lithium-ion batteries, which can more accurately describe the temperature distribution and obtain more details of the temperature field during battery use. Xiao et al.[27] constructed the state-space model of the nonintegral derivative of lithium-ion battery. The results are significant in reducing the computation and improving estimation precision.

With the continuous in-depth research of battery modeling and parameter identification by domestic and foreign scholars in the field, the type and accuracy of the model have been guaranteed to a certain extent.[27-34] Relevant representative modeling strategies include the finite-difference discrete modeling method[35] and reduced-order electrochemical modeling strategy[36] studied by Deng et al. In addition, Shi et al.[37] established a second-order lumped parameter electrical characteristic model based on the multitime scale effect of battery polarization internal resistance, and achieved high-precision identification of battery parameters through an asynchronous parameter identification strategy. Although relevant scholars and experts have studied the electrochemical model and equivalent circuit model of lithium-ion batteries innumerable, no one has carried out detailed work on lithium battery modeling and working condition verification based on the field of drones. Considering the high requirements of UAV work, the research work based on the equivalent circuit modeling and parameter identification of a UAV is particularly important.

Compared with the above transmission battery model, the electrochemical model according to the electrochemical reaction mechanism modeling, the model prediction precision is higher, and the estimate of the battery status is also more accurate, but the traditional high-precision pure electrochemical model has high computational complexity and many parameters need to be identified, which is currently difficult to implement in engineering. So this paper given the UAV lithium-ion battery accurately describe the goal of working status, comprehensively consider the accuracy and computational complexity of characterization, combined with the merits of different equivalent circuit model, using the combination of electrochemical and equivalent circuit and build the UAV lithium-ion battery splice-electrochemical polarization model (S-EPM). The S-EPM explains to a certain extent the polarization phenomenon caused by the electrochemical reaction speed on the positive and negative electrodes being slower than the electron movement speed, which greatly increases the fidelity of battery modeling. In addition, the paper discusses the least-squares optimal iterative theory based on a prior generalized inverse least-square (PGILS) method and realizes the full-parameter online identification in S-EPM based on this theory.

2 | MODEL FRAMEWORK

2.1 | Splice-electrochemical polarization modeling

The electrochemical model can realize the characterization of the battery state to a certain extent, but its modeling is more complicated, and many parameters that need to be identified, so it is not suitable for application in actual scenarios. Typical electrochemical models mainly include the Shepherd model, the Unnewhehr universal model, and the Nernst model. Several early electrochemical modeling methods in different forms are introduced in reference.[38]

The mathematical description of the Shepherd model is shown in Equation (1).

$$U_{\mathrm{L}}(k) = E_0 - RI(k) - K_1/SoC(k). \tag{1}$$

The mathematical description of the Unnewhehr universal model is shown in Equation (1).

$$U_{\mathrm{L}}(k) = E_0 - RI(k) - K_1 SoC(k). \tag{2}$$

The mathematical description of the Nernst model is shown in Equation (3).

$$\begin{aligned} U_{\mathrm{L}}(k) = E_0 - RI(k) - K_2 \ln[SoC(k)] \\ + K_3 \ln[1 - SoC(k)]. \end{aligned} \tag{3}$$

In Equations (1)–(3), $U_{\mathrm{L}}(k)$ is the output voltage at time k, E_0 is the open-circuit voltage (OCV) when SoC equals 1, R is the internal resistance of the cell, and K_1, K_2, and K_3 are constants chosen to make the model fit the data well. In addition, Plett et al.[38] and Wang et al.[39] show that all terms in these models can be recollected to form a "combined model" that performs better than any of the individual models. On the basis of the above modeling ideas, a new type of UAV lithium battery S-EPM is constructed by combining the Thevenin model with the combined model. By considering the influence of multiple coupling factors inside the lithium-ion battery, the purpose of high-fidelity modeling of the UAV lithium battery is achieved. The structure of S-EPM is shown in Figure 1.

In Figure 1, R_0 is the ohmic internal resistance. Through this parameter, the transient voltage drop at both ends of the positive and negative poles caused by the ohmic effect in the charging and discharging process of lithium-ion batteries is characterized. The first-order resistor–capacitor (RC) parallel circuit is used to characterize the relaxation effect of the battery, and then the transient response of the battery is expressed. R_{p}
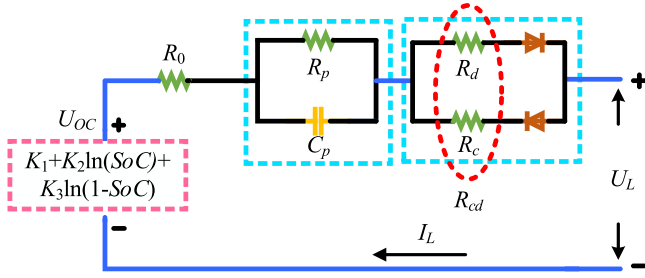
FIGURE 1 S-EPM model structure diagram. S-EPM, splice-electrochemical polarization model; SoC, state of charge.

represents the polarization resistance of the lithium-ion battery, and C_p represents the polarization capacitance of the lithium-ion battery. The parallel circuit composed of R_p and C_p reflects the generation and elimination of the polarization effect of the lithium-ion battery. R_d is the internal resistance during discharge, which characterizes the difference in the internal resistance of UAV lithium-ion batteries during discharge. R_{cd} represents the difference in internal resistance between the charged and discharged states of the battery. Among them, R_c is the internal resistance in the charged state, and its physical meaning is the internal resistance when the battery is fully charged. R_d is the internal resistance in the discharged state, and its physical meaning is the internal resistance after the battery is fully discharged. Generally speaking, the internal resistance in the discharged state is not stable and is too large; the internal resistance in the charged state is smaller and the resistance value is relatively stable. When the drone's lithium-ion battery is fully discharged, set R_{cd} equal to R_d, and when the drone's lithium-ion battery is fully charged, set R_{cd} equal to R_c. The identification results of the two in this paper are the average value, which is a fixed value. $U_{oc} - SoC$ is described by the combined model for SoC. Experiments show that the combined model can provide a better fitting effect in the whole charging and discharging process.

2.2 | Model-based state-space representation

Early electrochemical models need to identify many parameters, which makes the computational complexity of modeling high. The combined model adopted in this paper can reduce the parameters that need to be identified in the electrochemical model. In addition, the unknowns K_1, K_2, and K_3 in the combined model can be estimated by a simple system identification procedure, thereby reducing the computational complexity of the

modeling and ensuring that the model has high accuracy. On the basis of the structure of the S-EPM circuit, using Kirchhoff's circuit law, the state-space equation is established as shown in Equation (4).

$$
\begin{cases}
U_L(k) = U_{OC} - U_P(k) - I_L(k)R_0 - I_L(k)R_{cd}, \\
dU_p(k)/dk = I_L(k)/C_P - U_P(k)/C_P R_P, \\
U_{OC} = K_1 + K_2 \ln[SoC(k)] + K_3 \ln[1 - SoC(k)].
\end{cases}
\tag{4}
$$

The ideal voltage source in S-EPM is equivalent to the combined model, and its equivalent parameter value is represented by U_{oc}, representing the OCV of the battery. At the same time, the ohmic resistance of the battery is characterized by the resistance R_0. The physical meaning of the parameters in S-EPM is as follows:

1. The OCV value in the model is represented by the simplified Nernst equation.
2. The first-order RC parallel circuit is used to characterize the polarization effect.
3. The difference in the internal resistance of UAV lithium-ion batteries charge and discharge is characterized by R_d and R_c.

2.3 | PGILS parameter identification strategy

The above state-space equation is analyzed, and the differential of $U_p(k)$ in Equation (4) is replaced by the first-order backward difference, and the discretized equivalent differential is obtained as shown in Equation (5).

$$
\begin{aligned}
dU_p(k)/dk &\approx [U_p(kT) - U_p(k-1)T]/T \\
&= [U_p(k) - U_p(k-1)]/T.
\end{aligned}
\tag{5}
$$

In Equation (5), $U_p(k)$ and $U_p(k-1)$ are the voltage values across the polarization resistor at time k and time $k-1$, respectively. T is the system sampling period. It should be noted that considering the fastness and noise immunity, it is hoped that the sampling period should be as short as possible to reduce the influence of the pure lag of the system. However, considering the workload of the computer and the cost of the loop, the sampling period should be longer. Especially in multiloop control, each loop should have enough calculation time, which puts forward certain requirements for the selection of the sampling period. According to the selection basis of the sampling period described in Wang et al.,[40] combined with the existing hardware facilities of the laboratory, the

sampling period T in this paper is set to 1 s. It can not only ensure that the system has a long enough transition time, but also can make the computer reflect quickly through sampling, which improves the efficiency of algorithm iteration. Then, by substituting Equation (5) into Equation (4) the calculation equation of $U_p(k)$ is obtained, as shown in Equation (6).

$$U_P(k) = \frac{C_P R_P\{U_L(k) - U_L(k-1) + (R_0 + R_{cd})[I_L(k) - I_L(k-1)]\} + R_P I_L(k)T}{T}. \tag{6}$$

Substitute $U_p(k)$ in Equation (6) into Equation (4) to obtain the calculation equation of U_{oc}, and replace U_{oc} in Equation (4) with $K_1 + K_2\ln[SoC(k)] + K_3\ln[1 - SoC(k)]$, and the simplified discrete form of Equation (1) is shown in Equation (7).

$$\begin{aligned} U_L(k) = {} & x_1 + x_2 U_L(k-1) + x_3 \ln[SoC(k)] \\ & + x_4 \ln[1 - SoC(k)] + x_5 I_L(k) \\ & + x_6 I_L(k-1). \end{aligned} \tag{7}$$

In Equation (7), x_1, x_2, x_3, x_4, x_5, and x_6 are the coefficients of the discrete state-space equations, whose values can be solved by the least-squares estimation. The expansion forms of x_1, x_2, x_3, x_4, x_5, and x_6 are shown in Equation (8).

$$\begin{cases} x_1 = TK_1/(T + C_P R_P), \quad x_2 = C_P R_P/(T + C_P R_P), \\ x_3 = TK_2/(T + C_P R_P), \quad x_4 = TK_3/T + C_P R_P, \\ x_6 = \{C_P R_P(R_0 + R_{cd})\}/(T + C_P R_P), \\ x_5 = [C_P R_P(R_0 + R_{cd})]/(T + C_P R_P) \\ \qquad + [T(R_0 + R_P + R_{cd})]/(T + C_P R_P). \end{cases} \tag{8}$$

At this time, the parameters of the model are calculated as shown in Equation (9).

$$\begin{cases} K_1 = x_1/(1 - x_2), \quad K_2 = x_3/(1 - x_2), \\ K_3 = x_4/(1 - x_2), \quad R_f = R_{cd} + R_0 = x_6/x_2, \\ R_P = (x_2 x_5 + x_6)/(x_2^2 - x_2), \\ C_P = -x_2^2/(x_2 x_5 + x_6). \end{cases} \tag{9}$$

In Equation (9), R_f is the sum of the internal resistance of R_{cd} and R_0, and the parameter separation of R_c, R_d, and R_0 is achieved through the identification of R_f and the measurement result of the high-precision internal resistance tester.

In the process of UAV lithium-ion battery test, through the use of battery internal resistance tester

AT520B, implementation of UAV lithium-ion battery internal resistance measurement, the internal resistance testing equipment measuring range is 0.01 mΩ–300.00 Ω, the precision is 0.50%. Combined with the parameter identification results in Equation (9), the charge and discharge resistance R_{cd} in the S-EPM can be obtained.

Using the state-space equation in the discrete form of the model, based on the least-squares theory, the full-parameter online identification of the lithium-ion battery S-EPM is performed. According to Equation (9), through the state-space description in discrete form, an S-EPM exogenous autoregressive model based on a complete set of experiments is given, as shown in Equation (10).

$$\boldsymbol{Y} = \boldsymbol{A}\boldsymbol{X}$$
$$\Leftarrow \begin{cases} \boldsymbol{X} = [x_1, x_2, x_3, x_4, x_5, x_6]^T, \\ \boldsymbol{A} = \{\boldsymbol{A}_0, \boldsymbol{A}_1, \boldsymbol{A}_2, ..., \boldsymbol{A}_k, ..., \boldsymbol{A}_n\}, \\ \boldsymbol{Y} = [U_L(0), U_L(1), U_L(2), ..., U_L(k), ..., U_L(n)]^T, \\ \boldsymbol{A}_k = \{1, U_L(k-1), \ln[SoC(k)], \\ \qquad \ln[1 - SoC(k)], I_L(k), I_L(k-1)\}. \end{cases} \tag{10}$$

In Equation (10), k represents the current moment, $\boldsymbol{X}$ is the matrix of coefficients to be identified, and $\boldsymbol{A}$ is the matrix of independent variables. Its value is the set of key parameter data values, such as current and voltage obtained in the whole experiment. $\boldsymbol{A}_k$ is the data matrix under a single time interval, and $\boldsymbol{Y}$ is the output matrix composed of the entire experiment, also called the dependent variable matrix.

When performing online parameter identification of lithium batteries, due to the influence of computer data collection methods, the battery management system can only upload a set of data, such as current and voltage at a time, which is affected by the data collection mode, this paper further explores on the basis of the traditional recursive least-squares theory, and proposes a new type of least-squares algorithm based on a prior generalized inverse. The iterative process of the full-parameter online identification based on the PGILS algorithm is as follows.

Combine the dependent variable matrix $\boldsymbol{Y}$ in Equation (10) with the independent variable matrix $\boldsymbol{A}$, and then solve the coefficient matrix $\boldsymbol{X}$ to be identified, as shown in Equation (11).

$$X = X^{-1}Y \Rightarrow X = (A^TA)^{-1}A^TY. \tag{11}$$

According to the iterative calculation requirements, set the set of current, voltage, and other data before the k group as A_k, it is obvious that

$$\begin{cases} X_k = \left(\underbrace{A_k^T A_k}_{G_k} \right)^{-1} A_k^T Y_k, \\ X_{k+1} = \left(\underbrace{\begin{bmatrix} A_k \\ A_{k+1} \end{bmatrix}^T \begin{bmatrix} A_k \\ A_{k+1} \end{bmatrix}}_{G_{k+1}} \right)^{-1} \underbrace{\begin{bmatrix} A_k \\ A_{k+1} \end{bmatrix}^T \begin{bmatrix} Y_k \\ Y_{k+1} \end{bmatrix}}_{M_{k+1}}. \end{cases} \tag{12}$$

In Equation (12), the matrix A_k is a set consisting of the first k groups of experimental data, and A_{k+1} is the $k+1$th group of experimental data values. X_k is the to-be-identified coefficient matrix solved under the first k groups of current and voltage data, X_{k+1} is the coefficient matrix to be identified, which is solved after adding the $(k+1)$th group of data on the basis of X_k. G_k, G_{k+1}, and M_{k+1} are matrix operators used for the iteration of the PGILS algorithm. According to the description of the correlation matrix in X_0 and X_1 in Equation (12), the coupling relationship in the matrix operator in the calculation of PGILS algorithm iteration is deduced as shown below.

$$\begin{cases} G_k = G_{k+1} - A_{k+1}^T A_{k+1}, \\ M_{k+1} = G_k X_k + A_{k+1}^T Y_{k+1}. \end{cases} \tag{13}$$

Bring the G_k in Equation (13) into M_{k+1}, and merge and integrate the similar terms in the formula to obtain the expressions of G_{k+1} and M_{k+1} for iterative calculation of the PGILS algorithm are shown in Equation (14).

$$\begin{cases} G_{k+1} = G_k + A_{k+1}^T A_{k+1}, \\ M_{k+1} = G_{k+1} X_k + A_{k+1}^T (Y_{k+1} - A_{k+1} X_k). \end{cases} \tag{14}$$

According to the calculation result of Equation (14), G_{k+1} and M_{k+1} are, respectively, brought into Equation (12), and the coupling relationship between X_k and X_{k+1} is obtained, as shown in Equation (15).

$$X_{k+1} = X_k + G_{k+1}^{-1} A_{k+1}^T (Y_{k+1} - A_{k+1} X_k). \tag{15}$$

In Equation (15), from the perspective of optimal iteration, X_k is the original information in the optimal solution of parameter identification, also called old information, X_{k+1} is the new information after adding the data group, and the coupling relationship between

X_k and X_{k+1} clarifies that the PGILS algorithm uses the original information to modify the new information. In addition, the solution of the inverse matrix in engineering will take up a lot of computer resources, thereby reducing the utilization of data, so Equation (15) needs to be optimized, and the optimization steps are as follows.

Using the Sherman–Morrison–Woodbury formula, the form of G_{k+1}^{-1} in Equation (15) is optimized. Let G_k^{-1} and G_{k+1}^{-1} operators be P_k and P_{k+1}, respectively, and get the form shown in Equation (16).

$$P_{k+1} = P_k - P_k A_{k+1}^T \left(E + A_{k+1} P_k A_{k+1}^T \right)^{-1} A_{k+1} P_k. \tag{16}$$

In the battery management system, since the computer can only collect a set of data, such as current and voltage at a time, Equation (16) can be optimized into the following form.

$$P_{k+1} = P_k - \left(P_k A_{k+1}^T A_{k+1} P_k \right) / \left(1 + A_{k+1} P_k A_{k+1}^T \right). \tag{17}$$

The PGILS algorithm introduces the Sherman–Morrison–Woodbury formula; this avoids the work of matrix inversion, greatly increases the efficiency of computer processing data, and makes the algorithm simple and easy to implement. After the above derivation, the derivation process of the PGILS algorithm is as follows.

(1) Using the generalized inverse to find the initial solution.

$$\begin{cases} X_0 = \left(A_0^T A_0 \right)^{-1} A_0^T Y_0, \\ P_0 = \left(A_0^T A_0 \right)^{-1}. \end{cases} \tag{18}$$

(2) Iteratively calculate the optimization operator matrix P_{k+1} and the error correction matrix ε_{k+1}.

$$\begin{cases} P_{k+1} = P_k - \dfrac{P_k A_{k+1}^T A_{k+1} P_k}{1 + A_{k+1} P_k A_{k+1}^T}, \\ \varepsilon_{k+1} = Y_{k+1} - A_{k+1} X_k. \end{cases} \tag{19}$$

(3) Iteratively update the gain matrix K_{k+1} and the coefficient matrix X_{k+1}.

$$\begin{cases} K_{k+1} = P_{k+1} A_{k+1}^T, \\ X_{k+1} = X_k + K_{k+1} \varepsilon_{k+1}. \end{cases} \tag{20}$$

(4) Iterative loop to the end of the entire time series.

It should be noted that when the SoC is used as a part of the model state, the precision of the SoC needs to be considered. The fitting curve for OCV-SoC can be obtained by fitting the experimental data. In the parameter identification of the model, this paper adopts a simple and effective method, which is to iteratively calculate the SoC value obtained by the ampere-hour integration as the current real SoC value. Although the SoC value obtained by the ampere-hour integration has errors, it also greatly reduces the computational complexity of the model. Future work will combine the above modeling strategies with SoC estimation. The SoC of the battery is estimated with high precision by using different estimators, and the value is returned to PGILS. This closed-loop iterative strategy can achieve a high-precision joint estimation of model parameters and the internal state of the battery. To show the pros and cons of the PIG algorithm more intuitively, the quantitative analysis indicators used in this paper are: RMSE, mean absolute percentage error (MAPE), and maximum error (MAXE), and the calculation is shown in Equation (21).

$$RMSE = \sqrt{\frac{1}{n}\sum_{i=1}^{n}(y_i - \hat{y}_i)^2},$$
$$MAPE = \frac{1}{n}\sum_{i=1}^{n}\frac{|y_i - \hat{y}_i|}{y_i} \times 100\%, \quad (21)$$
$$MAXE = Max|y_i - \hat{y}_i|.$$

In Equation (21), n represents the total time step. The y_i and $\hat{y}_i$, respectively, represent the measured value and estimated value of the terminal voltage.

3 | EXPERIMENTS AND RESULTS ANALYSIS

On the basis of the PGILS algorithm, the hybrid pulse power characterization (HPPC) experimental data is used to identify the full parameters of the model, and then the feasibility of S-EPM is verified through the target compound discharge rate test and the full-function charge–discharge test. The experimental results of multiple operating conditions show that the model has high accuracy.

3.1 | Test equipment and procedures

To verify the accuracy and fidelity of the S-EPM model, the UAV ternary polymer lithium-ion battery is selected as the experimental sample, based on the battery's high-precision internal resistance tester, battery high-power

charge and discharge tester, and temperature control box. The experimental platform is set up, as shown in Figure 2. The test is carried out at a constant temperature of 25°C. The rated capacity of the experimental monomer sample is 72 Ah. The battery charging steady-state internal resistance measured by the high-precision internal resistance tester is 0.67 mΩ, and the discharge steady-state internal resistance is 0.52 mΩ.

3.2 | HPPC test analysis

To identify the full parameters in the S-EPM, this paper carried out an HPPC test on the UAV lithium-ion battery samples. The experiment procedures have been described in detail in Shi et al.,[28] and the experimental results are shown in Figure 3. Among them, Figure 3A is the current single pulse curve of the HPPC test, Figure 3B is the current curve of the main charging HPPC test, Figure 3C is the voltage curve of the main charging HPPC test, and Figure 3D is the SoC curve of the HPPC test.

3.3 | Full-parameter identification results

On the basis of the abovementioned HPPC test, based on the coupling relationship between the parameters in S-EPM, combined with the optimal iterative strategy of PGILS, the full-parameter identification of S-EPM is realized. First, using experimental data, combining Equations (18) and (19), complete the iterative identification of the coefficient matrix A. Finally, the parameters of the belt identification result based on PGILS are separated by Equation (9) to realize the identification of the model parameters. The parameter identification results are shown in Figure 4.

Figure 4A–F, respectively, shows the identification result curves of K_1, K_2, K_3, R_f, R_p, and C_p in the S-EPM under the full-time series. Because the precision of the initial value of the method based on PGILS parameter identification is too high, this paper has carried out a second optimization in the selection of the initial value of the algorithm. That is, the initial value of the first iteration of the algorithm is the initial value of the second iteration so that the parameter identification results after the second optimization have a higher degree of convergence.

In addition, as mentioned above, the charged internal resistance R_c and the discharged internal resistance R_d in the S-EPM have been measured by a high-precision internal resistance tester, and their values are $R_c = 0.67$ mΩ, $R_d = 0.52$ mΩ. According to Equation (9), $R_f = R_{cd} + R_0$, and then the value of R_0 can be calculated. To simplify the

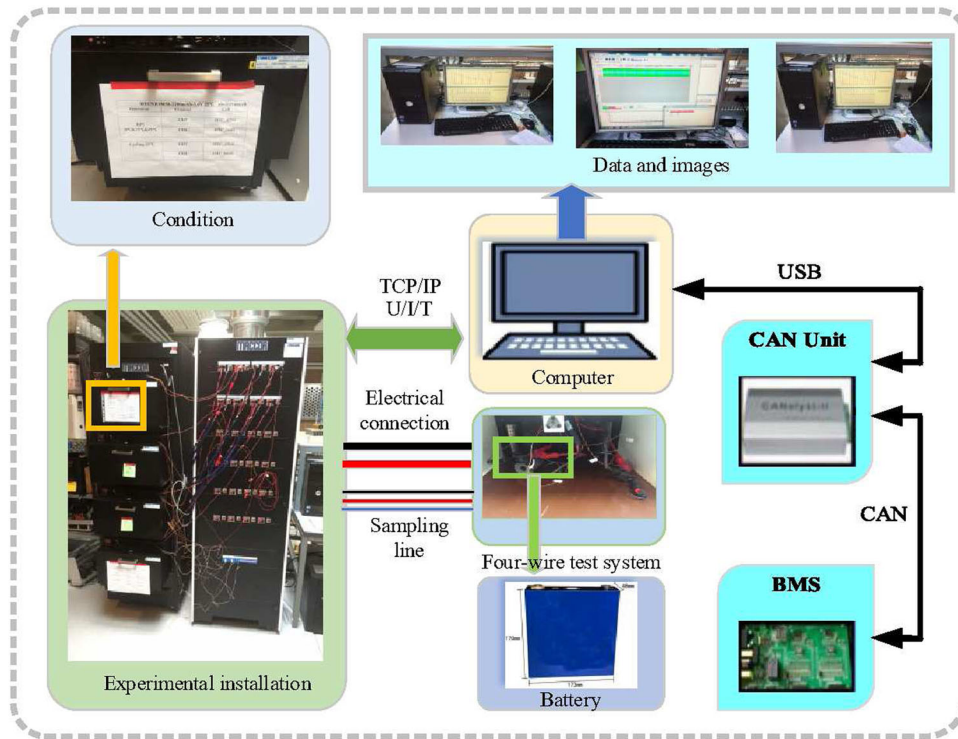**FIGURE 2** Test equipment appearance drawing. BMS, Battery Management System; CAN, Controller Area Network; IP, Internet Protocol; TCP, Transmission Control Protocol; USB, Universal Serial Bus.
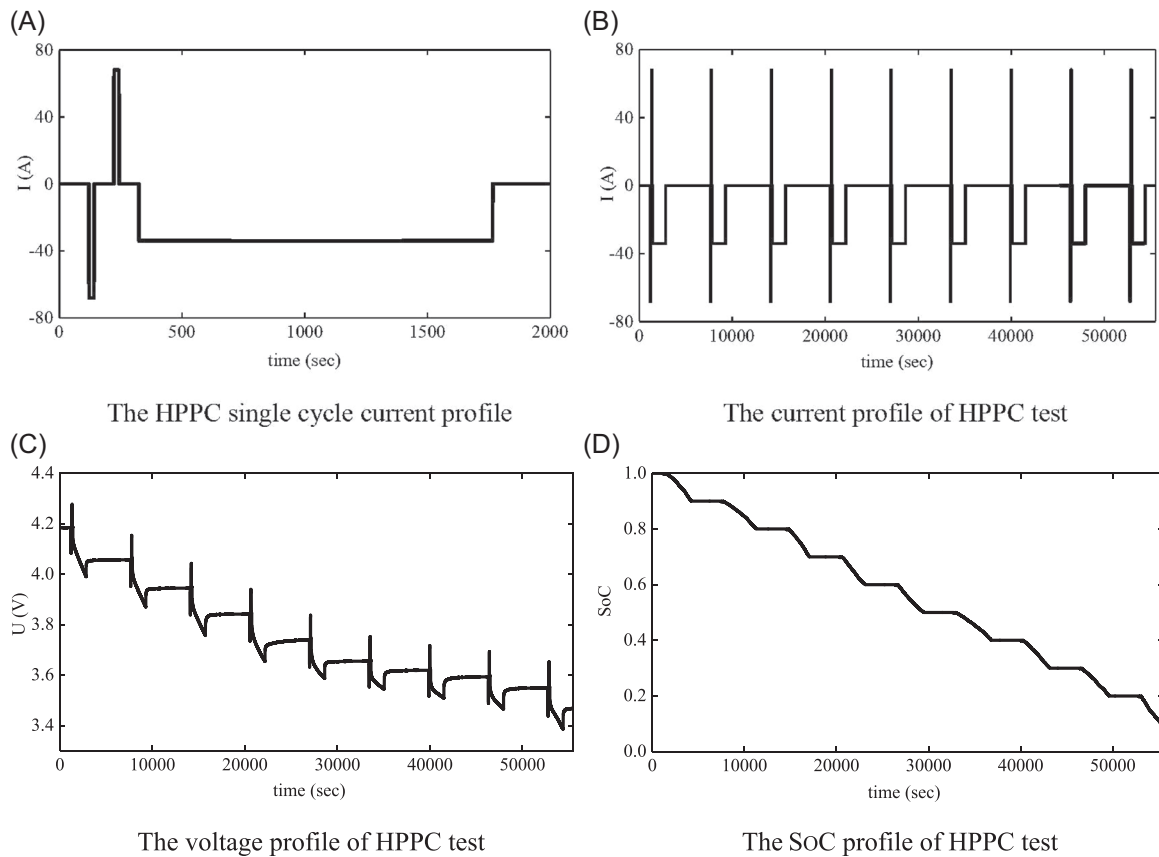

The HPPC single cycle current profile

The current profile of HPPC test

The voltage profile of HPPC test

The SoC profile of HPPC test

FIGURE 3 HPPC test index curves. HPPC, hybrid pulse power characterization; SoC, state of charge.

calculation, in this paper, the value of R_0 is averaged, and the average value is $R_0 = 0.61$ mΩ.

As can be seen from Figure 4G,H, the MAXE of the terminal voltage of the HPPC experiment does not exceed 0.4%, and the MAXE of terminal voltage does not exceed 0.3%. The experimental results effectively prove that S-EPM can well reflect the internal changes of UAV lithium-ion batteries.

(A) Identification result curve of K_1

(B) Identification result curve of K_2

(C) Identification result curve of K_3

(D) Identification result curve of R_f

(E) Identification result curve of R_p

(F) Identification result curve of C_p

(G) Terminal voltage comparison curve
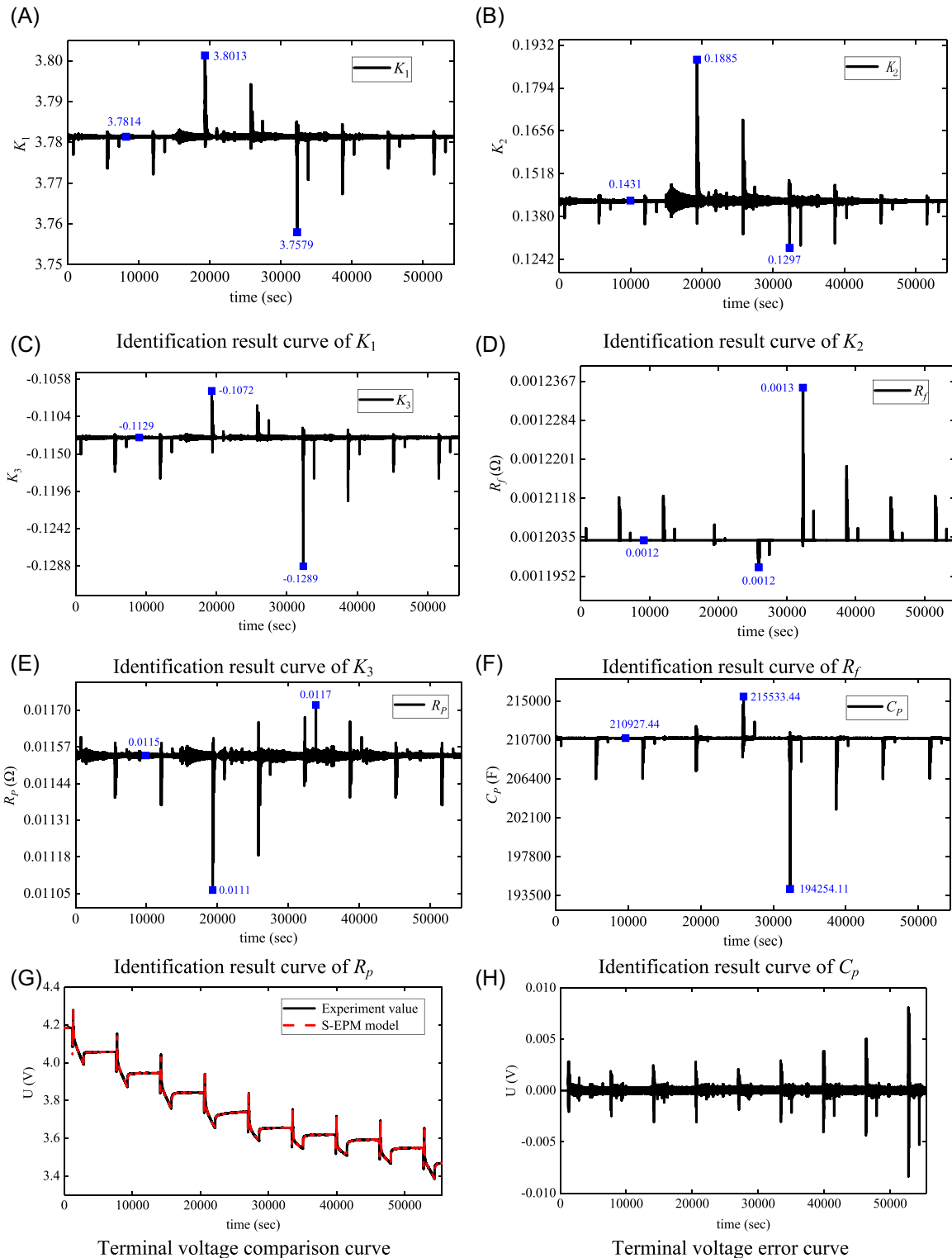
(H) Terminal voltage error curve

FIGURE 4 Full-parameter identification results and terminal voltage error curve

In the actual application of UAV BMS, in addition to the precision index of parameter identification, it is also necessary to consider the operating efficiency of the algorithm. The operation of the traditional least-squares algorithm relies heavily on the initial precision. If the initial value is given unreasonably, it may even diverge in the iterative process. To verify the operating efficiency of the PGILS algorithm, this paper gives the algorithm running time under different initialization conditions. This paper designs two sets of experiments with different initialization conditions. The first group is the initial value with higher

precision (its initial value is the convergence value after the algorithm iteration), and the second group is the initial value with lower precision (its initial value is 0). The running time of the algorithm under two different initialization conditions is shown in Table 1.

From the operating efficiency of the PGILS algorithm in Table 1, it can be seen that the algorithm running time under the same computer with different initial values is roughly the same. It can be concluded that the precision of the initial value has little effect on the running time of the PGILS algorithm. For this reason, when unmanned BMS is

Number of tests	First time	Second time	Third time	Fourth time	Fifth time
First group (s)	3.79797	3.076345	3.21761	3.60892	3.19987
Second group (s)	3.72011	3.48879	3.29567	3.10462	3.19822

TABLE 1 Running time of the algorithm at different initial values

Parameter	K_1	K_2	K_3	R_f	R_p	C_p
Number of iterations	85	113	98	575	587	583
Convergence time (s)	0.00156	0.00208	0.00180	0.01057	0.01079	0.0107

TABLE 2 Convergence time of each parameter under large error initial value

(A)

The current profile

(B)

The terminal voltage and SoC profiles

(C)

The terminal voltage contrast curve

(D)

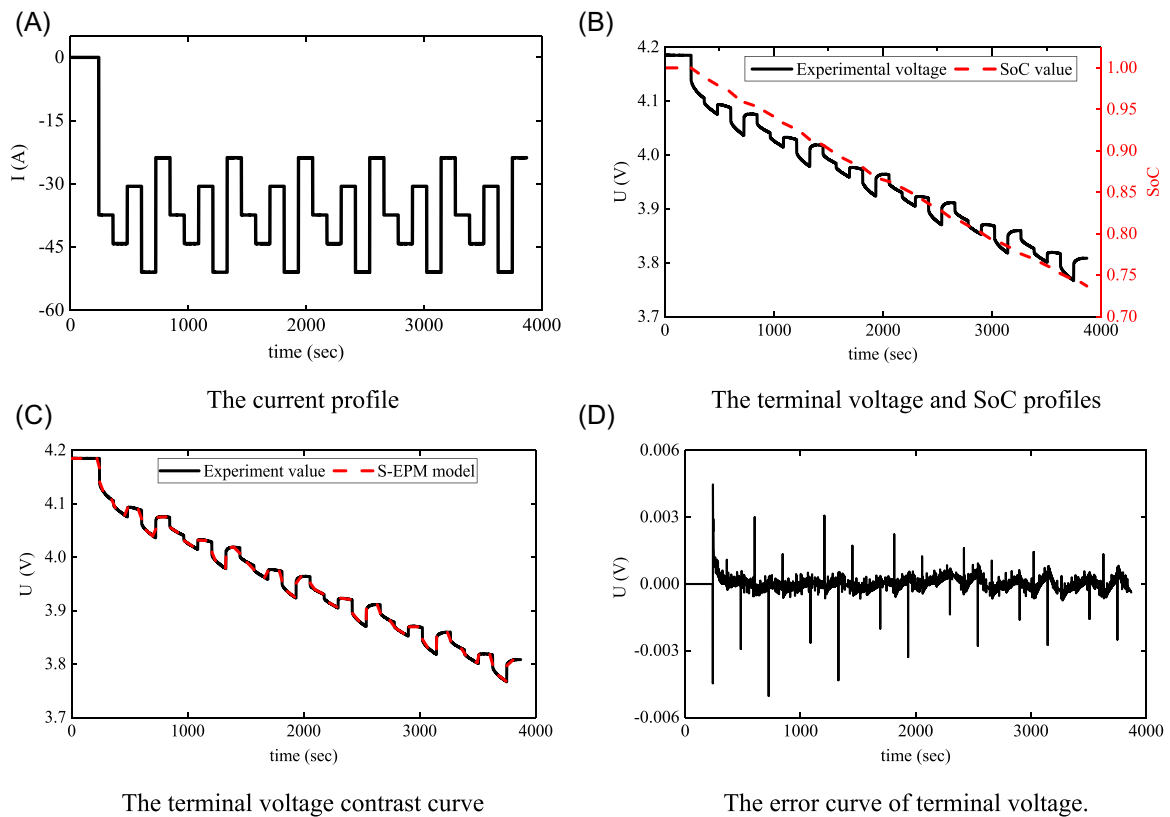The error curve of terminal voltage.

FIGURE 5 Targeted complex discharge rate test experiment result curve. SoC, state of charge.

used, it is possible to read historical data and initialize the algorithm without knowing the initial value.

To further explore the convergence speed of the algorithm, continue to study and analyze on the basis of the second set of experiments in Table 1. This paper takes the number of iterations required when the convergence error of each parameter is 5.00% and records it. Divide the number of iterations required for convergence by the total number of iterations to get the convergence time. The results are shown in Table 2.

Table 2 shows the number of iterations of each parameter when the algorithm is iterated to an error of 5% under a large initial value error. The number of iterations under the whole working condition is 54,414 times, and the convergence time is obtained. It can be seen from the table that the convergence speed of each parameter is extremely fast when the initialization error is large, all at the millisecond level, which further verifies that the algorithm has high operating efficiency.

3.4 | Targeted complex discharge rate test (TCDRT)

Owing to the complex application environment of UAV, a single HPPC experiment is not enough to fully prove the adaptability of the S-EPM to the external environment. To further verify the fidelity of S-EPM, this paper designs a TCDRT for UAVs on the premise of fully investigating the UAV's use environment and power requirements. In the experiment, the UAV lithium-ion battery sample was discharged with different rate combinations (0.35, 0.45, 0.55, 0.65, and 0.75 C), and the terminal voltage of the battery was tracked through S-EPM to simulate the battery based on S-EPM.

First, get the TCDRT experimental data according to the TCDRT experimental conditions. Then, using the above-mentioned S-EPM parameter identification method, combined with the full-parameter identification result shown in Figure 4, the terminal voltage comparison curve and the terminal voltage error curve under the TCDRT experiment are obtained, and the results are shown in Figure 5.

Figure 5A is the current curve of the TCDRT experiment, and Figure 5B is the voltage and SoC curve of the TCDRT experiment. Figure 5C is a comparison curve between the experimental value of the TCDRT experimental terminal voltage and the true value, and Figure 5D is the TCDRT experimental terminal voltage error curve. It can be seen from Figure 5C,D that the maximum voltage error of the UAV targeted S-EPM under the TCDRT experiment does not exceed 5.500 mV, and its MAXE does not exceed 0.200%, further verifying that the S-EPM has a high-fidelity degree.

3.5 | Full-function charging and discharging test (FFCDT)

To verify the adaptability of S-EPM, this paper designs an FFCDT according to the application environment of UAV. The experiment simulates the startup and unlocking of the drone during the flight and the power output of the drone in an emergency. On the basis of the lithium-ion battery samples selected in the previous paper, the UAV full-function charging and discharging experiment was carried out. The full-featured charging and discharging experiment process based on the UAV lithium-ion batteries sample is shown in Figure 6.

Before the UAV executes the flight mission, it first prestarts the crew. Its purpose is to complete the accurate calibration of various sensors in the crew to ensure that the UAV can start normally. This process is simulated by T_a in the FFCDT experiment. After the prestart is completed, the UAV is unlocked and the flight mission of the UAV is continued. This process is simulated by T_b
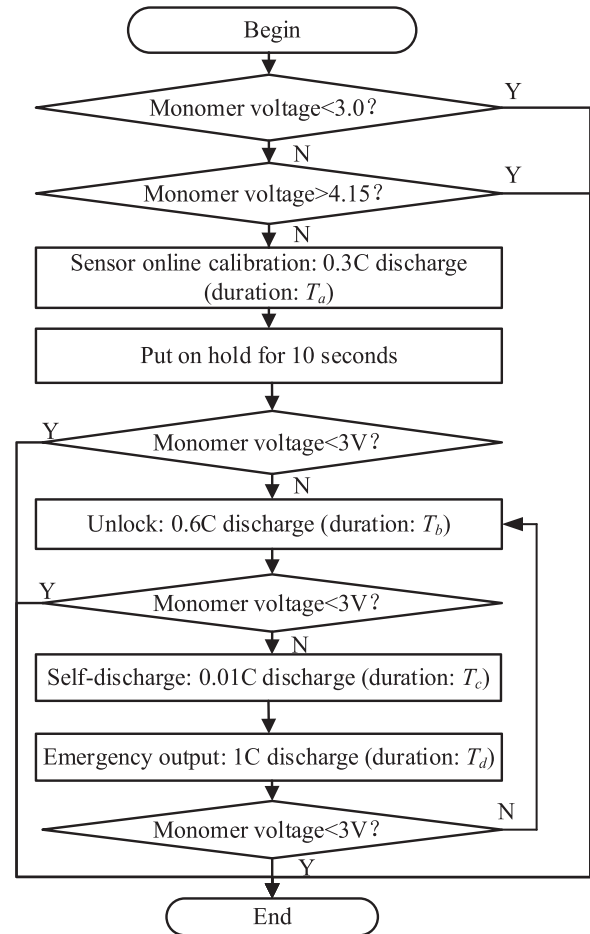

FIGURE 6 UAV full-function charge and discharge test experiment process. IC, incremental capacity; UAV, unmanned aerial vehicle.

(A) The current profile

(B) The terminal voltage and SoC profiles

(C) The terminal voltage contrast curve

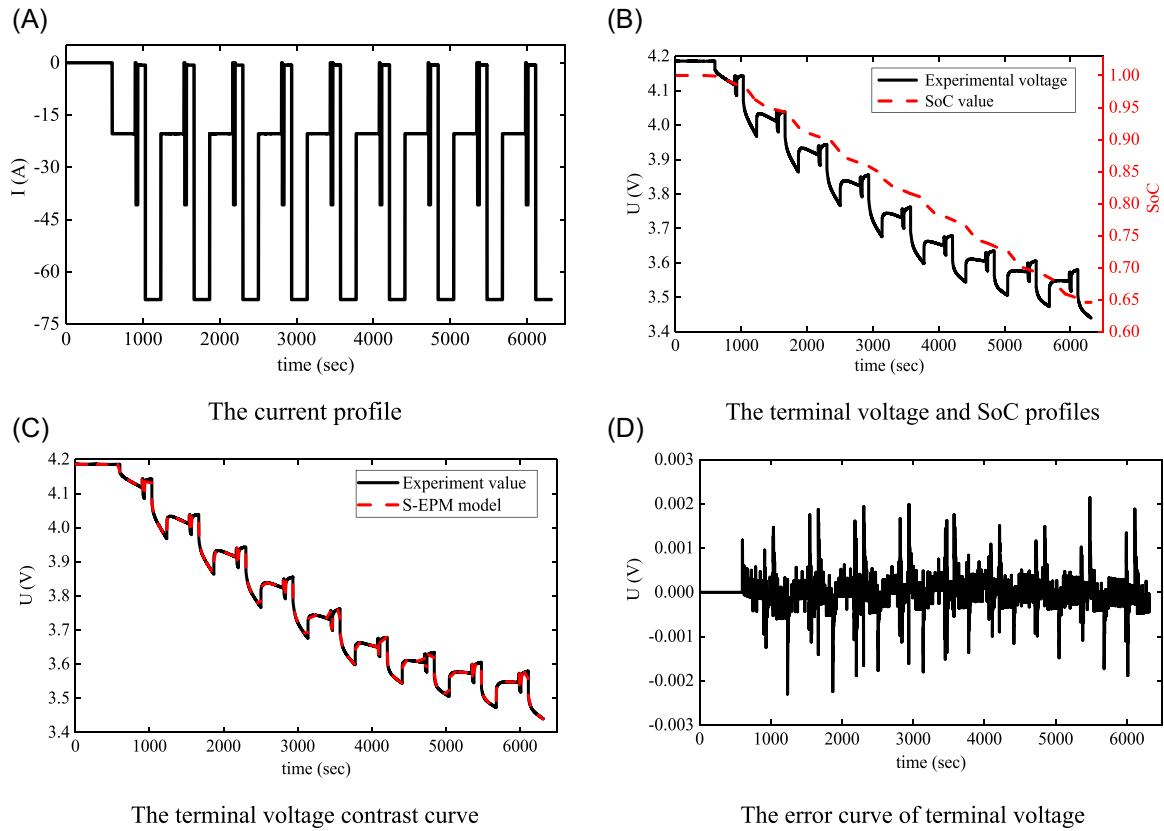(D) The error curve of terminal voltage

FIGURE 7 Phased working condition experiments index curves. S-EPM, splice-electrochemical polarization model; SoC, state of charge.

TABLE 3 Quantitative analysis of errors under different working conditions

Evaluation index	RMSE (mV)	MAPE (%)	MAXE (mV)
HPPC	0.200	0.003	8.367
TCDRT	0.352	0.006	5.022
FFCDT	0.302	0.005	2.300

Abbreviations: FFCDT, full-function charging and discharging test; HPPC, hybrid pulse power characterization; MAPE, mean absolute percentage error; MAXE, maximum error; RMSE, root-mean-square error; TCDRT, targeted complex discharge rate test.

in the FFCDT experiment. In addition, the battery self-discharge during the normal flight of the UAV cannot be ignored. This process is simulated by T_c in the FFCDT experiment. Considering the special application environment of the UAV, this paper adds the UAV emergency output simulation to the FFCDT experiment. This process is simulated by T_d in the FFCDT experiment.

On the basis of the FFCDT experiment flow chart in Figure 6, design the UAV targeted experimental conditions, where T_a is set to 600 s, T_b is 20 s, T_c is 100 s, T_d is 600 s. The entire operating condition is cycled 9 times,

thereby realizing the simulation of the UAV application process. According to the steps of the FFCDT experimental conditions, using the full-parameter identification results based on S-EPM, the terminal voltage comparison curve and the terminal voltage error curve under the FFCDT experiment are obtained, and the results are shown in Figure 7.

Figure 7A is the current curve of the FFCDT experiment, and Figure 7B is the voltage and SoC curve of the FFCDT experiment. Figure 7C is the comparison curve between the experimental value of the FFCDT experimental terminal voltage and the true value, and Figure 7D is the FFCDT experimental terminal voltage error curve. It can be seen from Figure 7C,D that the maximum voltage error of the UAV targeted S-EPM under the FFCDT experiment does not exceed 3 mV, and its MAXE does not exceed 0.07%. It fully demonstrates that S-EPM can adapt to the complex working environment of drones, and lays a model foundation for the follow-up research on the high-precision estimation of the SoC of the drone's lithium-ion battery.

To show the performance of the PGILS algorithm more intuitively, this paper carries out quantitative calculation and analysis of RMSE, MAPE, and MAXE

under HPPC and FFCDT conditions. The calculation results are shown in Table 3. It can be seen from Table 3 that the RMSE, MAPE, and MAXE under HPPC conditions are 0.200 mV, 0.003%, and 8.367 mV, respectively. The RMSE, MAPE, and MAXE under TCDRT conditions are 0.352 mV, 0.006%, and 5.022 mV, respectively. The RMSE, MAPE and MAXE under FFCDT conditions are 0.302 mV, 0.005%, and 2.300 mV, respectively. The maximum MAXE in the three working conditions is 2.633 mV less than in Shi et al.[28] (the MAXE of the terminal voltage is 11.000 mV). The maximum RMSE in the three working conditions is 8.348 mV less than that in Dai et al.[15] (the RMSE of the terminal voltage is 8.700 mV). It fully proves that the PGILS algorithm has high accuracy.

4 | CONCLUSION

This paper aims to establish a targeted high-fidelity equivalent circuit model of UAV. By considering the impact of the difference in charge and discharge internal resistance on battery modeling, a novel composite electrochemical polarization model for UAV lithium-ion batteries is proposed by combining the Thevenin model with the combined model. On the basis of the principle of the PGILSs method, combined with HPPC experimental data, the full-parameter identification in S-EPM is realized, which solves the shortcomings of traditional parameter identification methods that are time-consuming and large in error. The accuracy of the model is verified by the TCDRT and FFCDT. The voltage error of the model under each working condition is 5 and 3 mV, and the maximum percentage error ratio is 0.21% and 0.07%. The high fidelity of S-EPM is verified, and the model foundation is laid for the subsequent estimation of SoC of UAV lithium-ion batteries.

CONFLICT OF INTEREST
The authors declare no conflict of interest.

ORCID
Haotian Shi http://orcid.org/0000-0001-8120-8310
Shunli Wang http://orcid.org/0000-0003-0485-8082
Bobobee Etse Dablu http://orcid.org/0000-0003-0197-4766

REFERENCES

1. Wang YJ, Chen ZH. A framework for state-of-charge and remaining discharge time prediction using unscented particle filter. *Appl Energy*. 2020;260:114324.
2. Hu XS, Zou CF, Zhang CP. Technological developments in batteries. *IEEE Power Energy Mag*. 2017;15:20-31.
3. Ouyang MG, Du JY, Peng HE, Wang HW, Feng XN, Song ZY. Progress review of US–China joint research on advanced technologies for plug-in electric vehicles. *Sci China Technol Sci*. 2018;61:1431-1445.
4. Meng JH, Stroe DI, Ricco M, Luo GZ, Teodorescu R. A simplified mode based state-of-charge estimation approach for lithium-ion battery with dynamic linear model. *IEEE Trans Ind Electron*. 2019;66:7717-7727.
5. Amiribavandpour P, Shen WX, Mu DB. An improved theoretical electrochemical–thermal modeling of lithium-ion battery packs in electric vehicles. *J Power Sources*. 2015;284: 328-338.
6. Zhou S, Liu X, Hua Y, Zhou X, Yang S. Adaptive model parameter identification for lithium-ion batteries based on improved coupling hybrid adaptive particle swarm optimization-simulated annealing method. *J Power Sources*. 2021;482:228951.
7. Nejad S, Gladwin DT, Stone DA. A systematic review of lumped-parameter equivalent circuit models for real-time estimation of lithium-ion battery states. *J Power Sources*. 2016;316:183-196.
8. Ferahtia S, Djerioui A, Rezk H, Aissa C, Machmoum M. Optimal parameter identification strategy applied to lithium-ion battery model. *Int J Energy Res*. 2021;240(6):16741-16753.
9. Li C, Wang C, Cui N, Zhang C. Simplified electrochemical lithium-ion battery model with variable solid-phase diffusion and parameter identification over wide temperature range. *J Power Sources*. 2021;497(15):229900.
10. Yang S, Zhou S, Hua Y, Zhou X, Wu B. A parameter adaptive method for state of charge estimation of lithium-ion batteries with an improved extended Kalman filter. *Sci Rep*. 2021;11(1):5805.
11. Hu YR, Wang YY. Two time-scaled battery model identification with application to battery state estimation. *IEEE Trans Control Syst Technol*. 2015;23:1180-1188.
12. Jun M, Smith K, Graf P. State-space representation of Li-ion battery porous electrode impedance model with balanced model reduction. *J Power Sources*. 2015;273:1226-1236.
13. Li J, Wang D, Deng L, Cui Z, Pecht M. Aging modes analysis and physical parameter identification based on a simplified electrochemical model for lithium-ion batteries. *J Energy Storage*. 2020;31(6):101538.
14. Jiang Y, Xu J, Hou W, Mei X. A stack pressure based equivalent mechanical model of lithium-ion pouch batteries. *Energy*. 2021;221(5):119804.
15. Dai HF, Xu TJ, Zhu LT. Adaptive model parameter identification for large capacity Li-ion batteries on separated time scales. *Appl Energy*. 2016;181:119-131.
16. Wang D, Li X, Wang J, Zhang Q, Hao Z. Lithium-ion battery equivalent model over full-range state of charge based on electrochemical process simplification. *Electrochim Acta*. 2021;389:138698.

17. Tanaka T, Ito S, Muramatsu M. Accurate and versatile simulation of transient voltage profile of lithium-ion secondary battery employing internal equivalent electric circuit. *Appl Energy*. 2015;143:200-210.

18. Zhu R, Duan B, Zhang J, Zhang Q, Zhang C. Co-estimation of model parameters and state-of-charge for lithium-ion batteries with recursive restricted total least squares and unscented Kalman filter. *Appl Energy*. 2020;277:115494.

19. Jenkins B, Krupadanam A, Annaswamy AM. Fast adaptive observers for battery management systems. *IEEE Trans Control Syst Technol*. 2020;28:776-789.

20. Wu HJ, Yuan SF, Zhang X. Model parameter estimation approach based on incremental analysis for lithium-ion batteries without using open circuit voltage. *J Power Sources*. 2015;287:108-118.

21. Wei ZB, Zhao JY, Zou CF, Lim TM, Tseng KJ. Comparative study of methods for integrated model identification and state of charge estimation of lithium-ion battery. *J Power Sources*. 2018;402:189-197.

22. Kornas T, Wittmann D, Daub R, et al. Multi-criteria optimization in the production of lithium-ion batteries. *Procedia Manuf*. 2020;43:720-727.

23. Park J, Kim K, Park S, Baek J, Kim J. Complementary cooperative SoC/capacity estimator based on the discrete variational derivative combined with the DEKF for electric power applications. *Energy*. 2021;232:121023.

24. Tian JQ, Xu R, Wang YJ, Chen ZH. Capacity attenuation mechanism modeling and health assessment of lithium-ion batteries. *Energy*. 2021;221:119682.

25. Yuan SF, Wu HJ, Ma XR. Stability analysis for Li-ion battery model parameters and state of charge estimation by measurement uncertainty consideration. *Energies*. 2015;8:7729-7751.

26. Xie Y, Li W, Hu X, Lin X, Yue H. An enhanced online temperature estimation for lithium-ion batteries. *IEEE Trans Transp Electrification*. 2020;6:375-390.

27. Xiao H, Cheng Z, Offer G. Finding a better fit for lithium ion batteries: a simple, novel, load dependent, modified equivalent circuit model and parameterization method. *J Power Sources*. 2020;484:229117.

28. Shi HT, Wang SL, Fernandez C, Yu CM, Fan YC, Cao W. Improved splice-electrochemical circuit polarization modeling and optimized dynamic functional multi-innovation least square parameter identification for lithium-ion batteries. *Int J Energy Res*. 2021;5:1-15.

29. Zhou X, Huang J. Impedance-based diagnosis of lithium ion batteries: identification of physical parameters using multi-output relevance vector regression. *J Energy Storage*. 2020;31:101629.

30. Xu YDW, Xu JL, Yan XF. Lithium-ion battery state of charge and parameters joint estimation using cubature Kalman filter and particle filter. *J Power Electron*. 2020;20:292-307.

31. Tian JP, Xiong R, Yu QQ. Fractional-order model-based incremental capacity analysis for degradation state recognition of lithium-ion batteries. *IEEE Trans Ind Electron*. 2019;66:1576-1584.

32. Guo F, Hu GD, Zhou PK, Hu JY, Sai YH. State of charge estimation in electric vehicles at various ambient temperatures. *Int J Energy Res*. 2020;44:7357-7370.

33. Wang SL, Fernandez C, Liu XH, Su J, Xie YX. The parameter identification method study of the splice equivalent circuit model for the aerial lithium-ion battery pack. *Meas Control*. 2018;51:125-137.

34. Xu W, Xu JL, Liu BL, Liu JJ, Yan XF. A multi-timescale adaptive dual particle filter for state of charge estimation of lithium-ion batteries considering temperature effect. *Energy Sci Eng*. 2020;8:2784-2798.

35. Deng ZW, Hu XS, Lin XK, Kim Y, Li JC. Sensitivity analysis and joint estimation of parameters and states for all-solid-state batterie. *IEEE Trans Transp Electrification*. 2021;7:1314-1323.

36. Deng ZW, Hu XS, Lin XK, Xu L, Li JC, Guo WC. A reduced-order electrochemical model for all-solid-state batteries. *IEEE Trans Transp Electrification*. 2021;7:464-473.

37. Shi HT, Wang SL, Wang LP, et al. On-line adaptive asynchronous parameter identification of lumped electrical characteristic model for vehicle lithium-ion battery considering multi-time scale effects. *J Power Sources*. 2022;515:230725.

38. Plett GL. Extended Kalman filtering for battery management systems of LiPB based HEV battery packs: part 2. Modeling and identification. *J Power Sources*. 2004;134:262-276.

39. Wang YJ, Liu C, Pan R, Chen ZH. Modeling and state-of-charge prediction of lithium-ion battery and ultracapacitor hybrids with a co-estimator. *Energy*. 2017;121:739-750.

40. Wang YJ, Zhang X, Liu C, Pan R, Chen ZH. Multi-timescale power and energy assessment of lithium-ion battery and supercapacitor hybrid system using extended Kalman filter. *J Power Sources*. 2018;389:93-105.